THE JOURNAL OF PHYSICAL CHEMISTRY C

pubs.acs.org/JPCC

Article

Tuning the Optical Characteristics of Diketopyrrolopyrrole Molecules in the Solid State by Alkyl Side Chains

Published as part of The Journal of Physical Chemistry virtual special issue "Josef Michl Festschrift".

Bart W. H. Saes, Martin Lutz, Martijn M. Wienk, Stefan C. J. Meskers,* and René A. J. Janssen*

Cite This: *J. Phys. Chem. C* 2020, 124, 25229–25238

Read Online

ACCESS | Metrics & More | Article Recommendations | Supporting Information

ABSTRACT: The optical properties of two sets of donor–acceptor–donor molecules with terminal bithiophene donor units and a central diketopyrrolopyrrole (DPP) acceptor unit are studied. The two sets differ in the alkyl chains on the DPP, which are either branched at the α-carbon (3-pentyl) (**1**–**4**) or linear (*n*-hexyl) (**5**–**8**). Within each set, the molecules differ by the absence or presence of *n*-hexyl chains on the terminal thiophene rings in the 3′, 4′, or 5′ positions. While in solution, the optical spectra differ only subtly; they differ dramatically in the solid state. In contrast to **5**–**8**, **1**–**4** are nonplanar as a consequence of the sterically demanding 3-pentyl groups, which inhibit π-stacking of the DPP units. Using the crystal structures of **2** (brick layer stacking) and **6** (slipped stacking), we quantitatively explain the solid state absorption spectra. By computing the molecular transition charge density and solving the dispersion relation, the optical absorption of the molecules in the crystal is predicted and in agreement with experiments. For **2**, a single resonance frequency is obtained, while for **6** two transitions are seen, with the lower-energy transition being less intense. The results demonstrate how subtle changes in substitution exert large effects in optical properties.

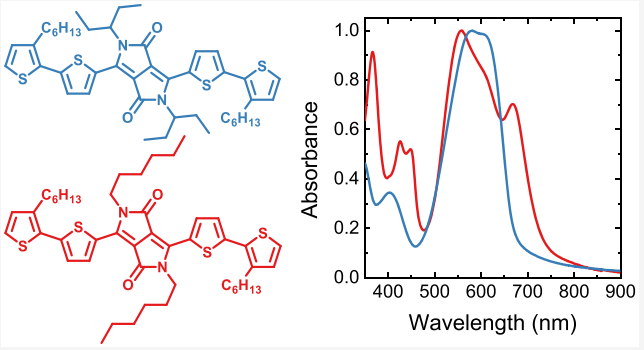

1. INTRODUCTION

Diketopyrrolopyrrole (DPP) based molecules and polymers attract considerable attention for a variety of applications, e.g., as pigments, in organic solar cells, organic field-effect transistors, as fluorescent probes, and in photodynamic and photothermal therapy.[1−12] DPP derivatives have a characteristic intense low-energy optical absorption and high charge carrier mobility. They can be conveniently synthesized and offer flexibility in terms of introducing different side chains and functional groups, which enables tailoring of their optical and electronic properties. The low-energy optical absorption of DPP molecules arises from their extended π-conjugation and the donor–acceptor interaction between the aromatic heterocycles that are adjacent to the DPP units.

DPP derivatives tend to aggregate strongly through π–π stacking interactions. To enable solution processing, the DPP derivatives are generally appended with linear or branched solubilizing side chains at the 2,5-*N*-lactam positions. The use of bulky side chains with high spatial density oriented perpendicular to the DPP plane reduces or even inhibits the aggregation behavior.[13] Alkyl chains that are introduced on the DPP moieties or on accompanying heterocycles generally have a small effect on the optical properties in solution. Yet, they strongly affect the absorption and emission spectra in the solid state as they influence the three-dimensional packing of the chromophores.[14−18] Such effects, known as crystallochromy,[19] have been explained using tight-binding extended Hückel calculations on infinite stacks[20] and in terms of exciton coupling based on the interaction between transition dipoles.[21] For DPP molecules with known crystal structures,[14,22−34] it possible to relate the optical and electronic properties to the three-dimensional packing. The relative orientation of adjacent molecules is particularly relevant regarding singlet-fission in which absorption of a photon by an assembly of two or more chromophores results in singlet excited state that decays via a spin-allowed formation of two triplet states.[35] Michl et al. have demonstrated the importance of intermolecular orientation in relation to the singlet fission rate.[36,37] Singlet fission has been identified for several DPP molecules.[27,28,32,38−43] For DPP-based molecules specifically, it is known that charge-transfer states between DPP units play a role in singlet fission and that

Received: August 11, 2020
Revised: October 25, 2020
Published: November 6, 2020

favorable relative orientations between minimally two chromophores are required for triplet formation.[32,44]

Here we investigate the role of the alkyl chains on the optical properties of two sets of DPP derivatives with terminal bithiophene donor units (Figure 1). The two sets differ in the

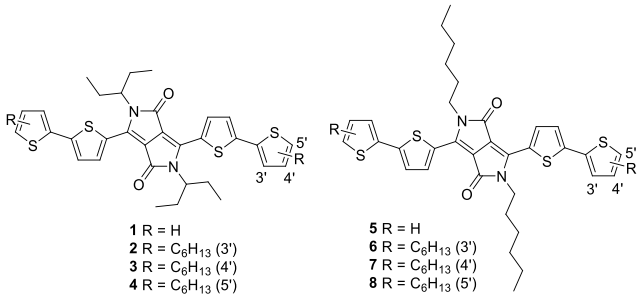

Figure 1. Molecular structures of TT-DPP-TT derivatives (**1**−**8**).

alkyl chains on the DPP, which are either branched at the α-carbon (3-pentyl) (**1**−**4**) or linear (*n*-hexyl) (**5**−**8**). The 3-pentyl substituent is sterically much more demanding than the linear *n*-hexyl chain, which was expected to change the molecular conformation and packing in the solid state. Within each set the molecules differ further by the absence or presence of *n*-hexyl chains on the terminal thiophene rings in the 3′, 4′, or 5′ positions. We find that while the absorption and emission spectra differ only slightly in solution, the spectra are markedly different in solid films. Using the crystal structures of representative molecules from each set, **2** and **6**, we show that simple arguments based on the orientation of nearest neighbor molecules in terms of J or H aggregates cannot explain the spectra. Instead, by summing all contributions to the total transition dipole and solving the dispersion relation, the optical absorption of the molecules in the crystal is predicted and in agreement with experiments. The main difference is caused by the sterically demanding 3-pentyl group in **2** that precludes π-stacking of the DPP core, resulting in a brick layer stacking of **2** in the solid state, while for **6** a slipped cofacial π-stacking arrangement occurs.

EXPERIMENTAL SECTION

Tris(dibenzylideneacetone)dipalladium ($Pd_2(dba)_3$) (Strem Chemicals Inc.), 2-bromo-3-hexylthiophene (TCI Chemicals), 2-bromo-4-hexylthiophene (TCI Chemicals), and 2-bromo-5-hexylthiophene (Merck) were used to synthesize stannylthiophene derivatives; thienyl boronic acids (4,4,5,5-tetramethyl-2-(thiophen-2-yl)-1,3,2-dioxaborolane (Merck), 2-(3-hexylthiophen-2-yl)-4,4,5,5-tetramethyl-1,3,2-dioxaborolane (TCI Chemicals), 2-(4-hexylthiophen-2-yl)-4,4,5,5-tetramethyl-1,3,2-dioxaborolane (TCI Chemicals), and 2-(5-hexylthiophen-2-yl)-4,4,5,5-tetramethyl-1,3,2-dioxaborolane (Merck)) and 3-bromopentane (Merck) were used as received. Triphenylphosphine (PPh_3) (AK Scientific) was recrystallized from absolute ethanol. *N*-Bromosuccinimide (NBS) (Merck) was recrystallized from water. 3,6-Di(thiophen-2-yl)-2,5-dihydropyrrolo[3,4-*c*]pyrrole-1,4-dione was synthesized according to literature procedures.[45] Dry solvents were obtained from a solvent purification system. The detailed synthetic procedures are described in the Supporting Information.

^{1}H and ^{13}C NMR spectra were recorded at, respectively, 400 and 100 MHz on a Bruker Avance III spectrometer at 25 °C. Molecular weights were determined using matrix-assisted laser desorption ionization-time-of-flight (MALDI-TOF) mass spectrometry (Bruker Autoflex Speed spectrometer). Melting points were taken on a Büchi Melting Point B-540 melting point apparatus and are uncorrected.

UV−vis-NIR spectra were measured using a PerkinElmer Lambda 1050 spectrophotometer equipped with a 3D WB PMT/InGaAs/PbS detector module. Emission spectra were recorded on an Edinburgh Instruments FS920 double-monochromator spectrophotometer equipped with a red sensitive photomultiplier (Hamamatsu R928P) operating at −20 °C and a nitrogen cooled near-IR sensitive photomultiplier (Hamamatsu R5509-73) operating at −80 °C. Time-resolved photoluminescence measurements were performed on an Edinburgh Instruments LifeSpec-PS spectrophotometer with excitation at 405 nm.

MM2 and DFT calculations were performed with the ADF (Amsterdam Density Functional) program.[46] The DFT calculations used the local density approximation and the Slater type orbital basis set STO DZ fc. Allowed optical transitions were calculated using the Davidson method from the ground state geometry. The lowest excited state involves mainly (>95%) one electron configuration with HOMO → LUMO one-electron excitation. Transition charge densities of the molecular transition are represented by a set of point charges located at the nucleus of each atom. The point charge at an atom was calculated by multiplying the coefficients for a particular atomic orbital in HOMO and LUMO at that atom and summing over all atomic orbitals. The point charges were positioned at the nuclei of the respective atoms.

The diffraction experiment was performed on a Bruker Kappa ApexII diffractometer with a sealed tube and Triumph monochromator (λ = 0.71073 Å) at a temperature of 150(2) K up to a resolution of $(\sin\theta/\lambda)_{max}$ = 0.65 Å^{-1}. Further details on the crystal structure determination can be found in the Supporting Information.

RESULTS AND DISCUSSION

Synthesis. Molecules **1**−**8** were synthesized in three steps from 3,6-di(thiophen-2-yl)-2,5-dihydropyrrolo[3,4-*c*]pyrrole-1,4-dione[45] by alkylation, bromination, and a palladium catalyzed cross-coupling reaction (Scheme 1). Compound **8** has been described previously, where it was synthesized via a somewhat different route.[47] The yield of the alkylation reaction where the 3-pentyl substituents, i.e., α-branched side chains, are introduced to obtain **a** was ostensibly low (3.8%) compared to yields of up to 70% for β-branched alkyl chains

Scheme 1. Syntheses of DPP Derivatives 1−8

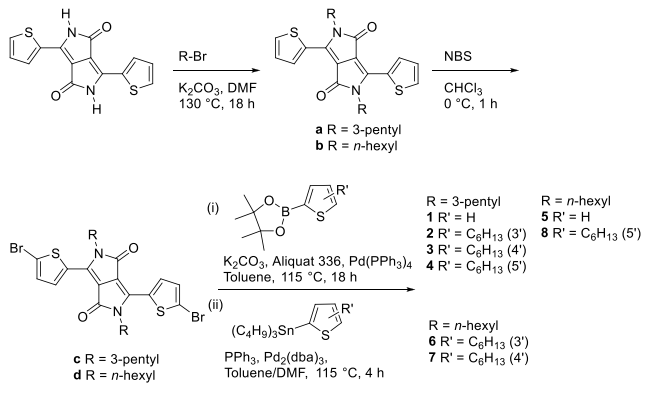

https://dx.doi.org/10.1021/acs.jpcc.0c07334
J. Phys. Chem. C 2020, 124, 25229−25238

and up to 80% found for linear, unbranched alkyl chains.[48] The low reaction yield for **a** is related to the use of a secondary bromoalkane, rather than a primary one and is typical for the synthesis of α-branched DPP molecules.[49] Subsequent bromination to **c** gave a yield of 86%. The yield of the bromination reaction with NBS is not strongly influenced by the branching of the alkyl side chain. The corresponding molecule with a linear hexyl side chain **d** was obtained from **b** as described previously.[50]

Molecules **1**−**8** were obtained from **c** and **d** in either Stille or Suzuki cross reactions. In our experience, coupling cross-coupling reactions involving thiophene derivatives proceed better via Stille than via Suzuki reactions.[51] Accordingly, **3** and **4** were successfully obtained via Stille cross-coupling of **c** with tributyl(4-hexylthiophen-2-yl)stannane and tributyl(5-hexylthiophen-2-yl)stannane, which were obtained following a literature procedure.[52] The attempted synthesis of **2** by Stille cross-coupling was, however, unsuccessful and resulted in a wide range of products. The reason for this failure is attributed to the inability to properly purify the oily (3-hexylthiophen-2-yl)stannyl derivative We decided to use Suzuki cross-coupling reactions for **1**, **2**, and **5**−**8**. The required boronic acids and esters are easier to purify and commercially available. As a general observation for these reactions, we found that crude reaction yields could be as high as >99%, but recrystallizing the materials sometimes proved difficult, dropping the yield to as low as 27%. Full details on the synthesis and characterization of the molecules by NMR and mass spectrometry can be found in the Supporting Information.

Optical Properties. The normalized UV−vis-NIR spectra (Figure 2a,b) of **1**−**8** in chloroform (CF) solution show a

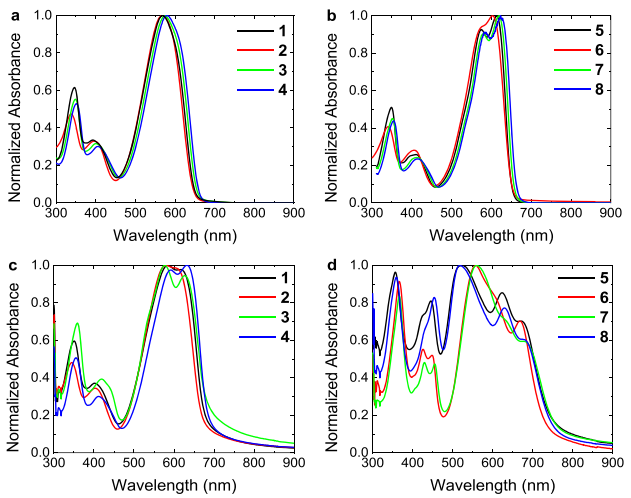

Figure 2. Normalized UV−vis-NIR spectra: (a) **1**−**4** in $CHCl_3$, (b) **5**−**8** in $CHCl_3$, (c) **1**−**4** as thin films, and (d) **5**−**8** as thin films.

strong π−π^* absorption band between 500 and 650 nm. The relevant spectral data are collected in Table 1. The interaction between the electron-rich thiophene rings and electron-deficient DPP moiety causes the π−π^* transition to have charge-transfer character. The 3-pentyl derivatives **1**−**4** show a largely unstructured band with a wavelength of maximum absorption (λ_{max}) of 573 ± 5 nm. In contrast, the *n*-hexyl derivatives **5**−**8** show two vibronic peaks at 615 ± 5 nm (0 ← 0) and 578 ± 3 nm (1 ← 0). The Huang−Rhys parameter (S) determined from the relative intensities of the vibronic peaks is between 0.90 and 0.95 and results in a prediction of a third vibronic peak with an intensity of 0.43, expected at around 545 nm. This transition is indeed visible in the spectra as a vague shoulder (Figure 2b). Also for the 3-pentyl derivatives **1**−**4**, a shoulder at longer wavelengths than λ_{max} is observed, hinting at an unresolved vibronic progression. From the intensity of the shoulder the Huang−Rhys parameter for **1**−**4** is estimated to be $S \approx 1.2$. As the Huang−Rhys parameter relates to the geometric distortion in the excited state, the distortion is larger for **1**−**4** than for **5**−**8**. Small Huang−Rhys parameters are generally associated with structurally defined molecules, and concomitantly, a larger Huang−Rhys parameter often represents a more distorted or flexible molecular geometry. The UV−vis-NIR spectra therefore suggest that the sterically demanding 3-pentyl chains on the DPP moiety cause a geometric distortion of the chromophore that is larger than that caused by *n*-hexyl chains.

For each set of molecules, the presence and position of the *n*-hexyl chain on the terminal thiophene rings also affects λ_{max}. In each case, λ_{max} increases going from 3′-hexyl, via 4′-hexyl, to 5′-hexyl substitution, with λ_{max} of the unsubstituted thiophene ring derivatives in between those of 3′ and 4′-hexyl (Table 1). This sequence results from a combination of electronic and steric effects. The electron donating hexyl substituents make the thiophene rings more electron rich and shift λ_{max} to longer wavelengths. The electronic effect is expected to be stronger for the 3′ and 5′ positions that are in conjugation with the DPP core and less for the 4′ position that is cross-conjugated. The fact that the λ_{max} of the 3′-hexyl derivatives is much lower than that of the 4′ and 5′ derivatives is ascribed to steric congestion of the terminal *n*-hexyl side chains with the conjugated backbone of **2** and **6**, which can result in a less planar molecular structure and decreases λ_{max} to values lower than those of **1** and **5**. For **6**, this geometric distortion is also reflected in the less-resolved vibronic coupling and having the higher intensity of the second vibronic peak in the absorption spectra compared to **5**, **7**, and **8**, pointing at a higher Huang−Rhys factor.

In thin films (Figure 2c,d), the UV−vis-NIR absorption spectra of the 3-pentyl derivatives **1**−**4** reveal two peaks of comparable intensity with maxima at 584 ± 6 nm and 620 ± 11 nm. The splitting can be due to vibrational coupling or exciton coupling or a superposition of these two effects.[53,54] For **1**−**3**, the peak at shorter wavelength is more intense, but for **4** the highest intensity is found at longer wavelengths. Like in solution, the absorption band redshifts going from 3′-hexyl, via 4′-hexyl, to the 5′-hexyl derivative in the solid state with the band of the unsubstituted derivative in between those of 3′ and 4′-hexyl. Overall, the spectral changes that occur for **1**−**4** when going from solution (Figure 2a) to the solid state (Figure 2c) are limited and suggest that no significant changes occur in the molecular geometry and that exciton coupling effects are moderate or have little net effect on the absorption spectrum.

In contrast, the UV−vis-NIR absorption spectra of thin films of the *n*-hexyl derivatives **5**−**8** (Figure 2d) strongly differ from the corresponding spectra in solution (Figure 2b). The spectra are much broader, show multiple peaks, and reach their highest intensity at shorter wavelength than the spectra in solution, while the peak at longest wavelength is significantly red-shifted and has the lowest intensity. While these are characteristics of H-aggregates, the long wavelength peak still has considerable intensity, indicating that the actual explanation is more complex. Previously, for molecules similar to **1**−**8**, yet with

https://dx.doi.org/10.1021/acs.jpcc.0c07334
J. Phys. Chem. C 2020, 124, 25229−25238

Table 1. Optical Characteristics of DPP Molecules 1−8

	absorption					fluorescence					
	solution		film			solution			film		
	λ (nm)	λ (nm)	λ (nm)	λ (nm)	λ (nm)	λ (nm)	λ (nm)	τ	λ (nm)	λ (nm)	τ
	(0 ← 0)	(1 ← 0)	1st	2nd	3rd	(0 → 0)	(0 → 1)	(ns)	(0 → 0)	(0 → 1)	(ps)
1		569	618	584		641	692[a]	2.16	670	723	54
2		568	603	581[a]		643	691[a]	2.27	678[a]	724	37
3		575	627	577		647	700[a]	2.02	672	720	42
4		581	632	592		655	705[a]	1.81	670	719	165
5	613	574	672	623	523	641	698	2.62		810[b]	
6	603	576[a]	668	665[a]	558	643	697[a]	2.72		810[b]	
7	620	579	678	629[a]	560	646	700	2.44		870[b]	
8	623	582	673	630	517	655	710	2.20		810[b]	

[a]Shoulder. [b]Very broad signal.

two 2′-ethylhexyl side chains on the DPP moiety, we found H-type aggregation when the *n*-hexyl chain is on the 4′-position, J-type aggregation for the 3′-position, and an intermediate situation or the molecule substituted at the 5′-position.[15] In the case of **5**−**8**, there is a clear tendency to form aggregates that feature a high wavelength absorption with a moderate intensity. The details of the intermolecular interaction and relative spatial organization seem to differ between **5** and **8** (λ_{max} = 520 ± 3 nm), and **6** and **7** (λ_{max} = 559 ± 1 nm).

We thus see clear differences in the UV−vis-NIR spectra of **1**−**4** and **5**−**8**. These are likely related to the fact that the linear *n*-hexyl is sterically less demanding than 3-pentyl substituents in **1**−**4**.

Photoluminescence (PL) spectra of solutions of **1**−**8** show a vibronically structured emission with the (0 → 0) transition at 646 ± 5 nm and the (0 → 1) peak at 699 ± 6 nm (Figure 3a,b and Table 1). In contrast to the absorption, the alkyl chain on DPP has virtually no effect on the position of the (0 → 0) emission but only affects the (0 → 1) band which is present as a shoulder for **1**−**4** and as a resolved peak for **5**−**8**. The Huang−Rhys factor for the emission spectra is marginally higher for **1**−**4** than for **5**−**8**. These similarities suggest that in the excited state the geometries of **1**−**8** are virtually identical. It is further remarkable that despite the minor differences in the position of the (0 → 0) bands between those of the 3-pentyl and the *n*-hexyl DPP derivatives, the positions differ more by the presence and position of the *n*-hexyl chain on the terminal thiophene rings because the pairs **1** and **5**, **2** and **6**, **3** and **7**, and **4** and **8** have identical wavelengths of maximum emission.

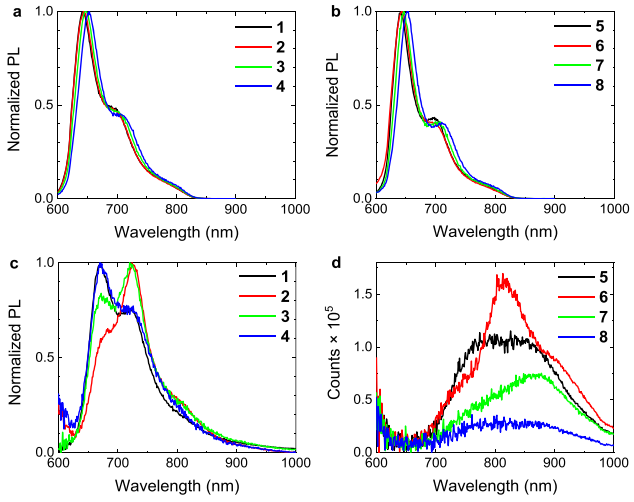

Figure 3. Fluorescence spectra: (a) **1**−**4** in $CHCl_3$, (b) **5**−**8** in $CHCl_3$, (c) **1**−**4** as thin films, and (d) **5**−**8** as thin films. Excitation wavelengths are 540 nm (a,b) and 550 nm (b,c). Spectra shown in panels a−c are normalized to enable direct comparison.

In thin films, the fluorescence of **1**−**4** is shifted to longer wavelengths by about 25 nm, and the spectral shape has changed (Figure 3c, Table 1). In each case two bands are visible, but their relative intensities differ. For **1** and **4**, the first peak at shorter wavelength is most intense, while for **2** and **3** the most intense peak is at longer wavelength. These differences in intensity may be related to differences in the coupling of transition dipole moments. For **5**−**8**, the fluorescence spectra in films differ dramatically from those in solution (Figure 3d). Weak, mostly unstructured broad bands in the 700−1000 nm region are observed. Such emission spectra are typical for strongly aggregated systems with a forbidden or weakly dipole-allowed lowest optical transition. In such a case, the emission is a slow and nonradiative decay, e.g., via exciton quenching, may occur.

Time-resolved fluorescence measurements on **1**−**8** in solution and thin film were used to determine excited-state lifetimes (Table 1, Figure 4). Similar excited state lifetimes were found for these molecules in $CHCl_3$, although they are slightly shorter for **1**−**4** (2.07 ± 0.17 ns) than for **5**−**8** (2.50 ± 0.20 ns). Also the presence and position of the *n*-hexyl chains has a remarkably consistent effect on the lifetime: τ(3′) > τ(unsubstituted) > τ(4′) > τ(5′) (Table 1). While the absolute differences are small, the consistent effects show that the origin of the differences lies in the details of the molecular structure. In thin films of **1**−**4**, the excited-state lifetime is reduced to the picosecond regime, with **4** having the slowest decay of around 165 ps. For **5**−**8**, the low fluorescence intensity precluded determining the lifetime.

Structural Properties. Crystals adequate for single crystal structure determination were obtained by vapor diffusion of cyclohexane into THF solutions of **2** and **6**. Repeatedly, crystallization attempts for **1**, **3**−**5**, **7**, and **8** under various conditions were unsuccessful. In **2** and **6**, the *n*-hexyl chain on the terminal thiophenes is in the 3′ position.

Molecule **2** crystallizes with one molecule (Z = 1) in a triclinic ($P\bar{1}$) unit cell. The molecule is positioned at the crystallographic inversion center. The torsion angle (Figure 5)

https://dx.doi.org/10.1021/acs.jpcc.0c07334
J. Phys. Chem. C 2020, 124, 25229−25238

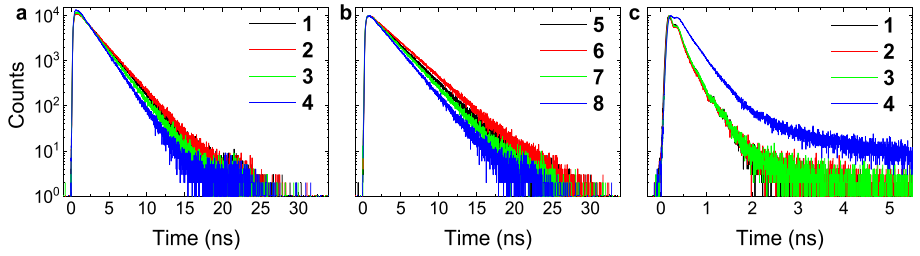

Figure 4. Time-resolved fluorescence: (a) **1**−**4** in chloroform, (b) **5**−**8** in chloroform, and (c) **1**−**4** in a thin film.

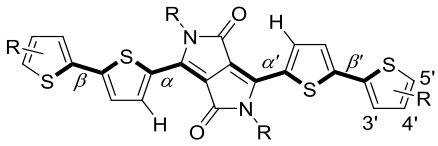

Figure 5. Definition of the torsion angles α, α', β, and β'. The signs were defined by looking from the termini to the center of the molecule.

around the bonds between the DPP unit and the adjacent thiophene rings α is −152.86(11)° (Table 2, Figure S1, Supporting Information), demonstrating a significant twist in the backbone as a consequence of the steric congestion of the 3-pentyl substituents on DPP. The torsion angle β around the bond between the two thiophene rings is +176.64(7)° (Table 2) and indicates a virtually coplanar bithiophene unit.

Table 2. Torsion Angles α and β in 2 and 6

	α	α'	β	β'
2[a]	−152.86(11)°		+176.64(7)°	
6′[a]	+176.3(4)°		−172.3(3)°	
6″	−173.0(4)°	+179.5(7)°	+173.4(3)°	+170.6(3)°

[a]Molecules **2** and **6′** are centrosymmetric

Molecule **6** crystallizes with three molecules ($Z = 3$) in the triclinic ($P\bar{1}$) unit cell. One of these (**6′**) is centered at the crystallographic inversion center, while the other two molecules (**6″**) have no internal symmetry but are identical by inversion symmetry (Figure S2, Supporting Information). The centrosymmetric molecule **6′** has α = +176.3(4)° and β = −172.3(3)°. The two symmetry-related molecules **6″** resemble the centrosymmetric molecule with α = −173.0(4)° and β = +173.4(3)° on one side and α' = +179.5(7)° and β' = +170.6(3)° on the other side. Hence, the torsion angles α and α' are significantly smaller in **6** than in **2**, pointing at a nearly coplanar thiophene-DPP-thiophene conjugated segment, although the torsion angles β and β' are slightly higher in **6** than in **2**. The main difference between **6′** and **6″** is the conformation of the *n*-hexyl chain at the DPP moiety (Figure S3, Supporting Information). For **6′**, the *n*-hexyl chain has an exclusive trans conformation, while in **6″** one of the two *n*-hexyl chains has a gauche conformation for the C(2)−C(3) bond.

^{1}H NMR spectroscopy indicates that the conformations of molecules **1**−**4** and **5**−**8** in solution are similar as found for **2** and **6** in the solid state. The α and α' angles of **6** deviate only a few degrees from planarity in the crystal (Table 2) and make that the hydrogen atom on the 3-position (H(3)) of the thiophene ring next to the DPP is close to the oxygen atom of the carbonyl group (Figure 5). In the crystal, these distances are 2.20 Å for **6′** and for **6″**, 2.26 and 2.19 Å. The near-coplanar structure and spatial proximity causes a downfield chemical shift of the H(3) protons to δ = 8.94 ± 0.05 ppm in the ^{1}H NMR spectra of **5**−**8** in $CHCl_3$ solution, compared to δ = 6.7−7.3 ppm for the other thiophene protons. The shift is due to an anisotropic induced magnetic field created by the neighboring carbonyl and is expected be the largest when the proton is in the plane of the DPP moiety. For **2** on the other hand, the oxygen−hydrogen distances in the crystal are longer (2.35 Å), and with α = −152.86(11)°, the protons are no longer in the plane spanned by the DPP. This nonplanar configuration is also reflected in the chemical shift of the H(3) protons, which is at δ = 8.55 ± 0.05 ppm in **1**−**4** and thus about 0.4 ppm upfield from the protons at the same position in **5**−**8**, while for the other thiophene protons δ is in the same range of 6.7−7.3 ppm for **1**−**4** as for **5**−**8**.

To investigate the differences in measured dihedral angles between the DPP segments and adjacent thiophene rings of **2** and **6**, force field (MM2) and density functional theory (DFT) calculations using the local density approximation (LDA) were performed. Using the crystallographic data as starting conformations, scans were performed for the torsion angle α for **2** and **6** (Figure 6). Both methods predict absolute potential minima for **2** at α = −160° and for **6** at α = ±180° that are very close to experimental torsion angles in the crystal structures. Hence, the calculations confirm a nonplanar structure for **2** and a virtually planar structure for **6**. Both methods predict local potential energy minima α = −25° and α = 30° for **2** and at α = −15° and α = 20° for **6**, separated by a local maximum in the energy close to α = 0°. The relative energies of the local minima match surprisingly well for the MM2 and DFT methods, but predicted rotational barriers differ significantly, approximately by a factor of 2.5. In any case, the rotation barrier is much higher than the thermal energy at room temperature, such that interconversion between the minima is not possible.

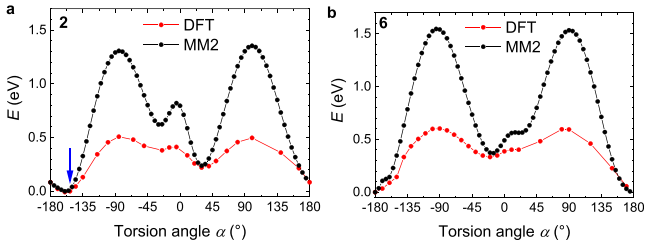

Figure 6. (a) Potential energy of **2** as a function of the torsion angle α calculated with DFT and MM2 force field (MM2 FF). The blue arrow indicates the α in the crystal structure and (b) same for **6**. In the crystal structure of **6**, α is close to ±180°.

https://dx.doi.org/10.1021/acs.jpcc.0c07334
J. Phys. Chem. C 2020, 124, 25229−25238

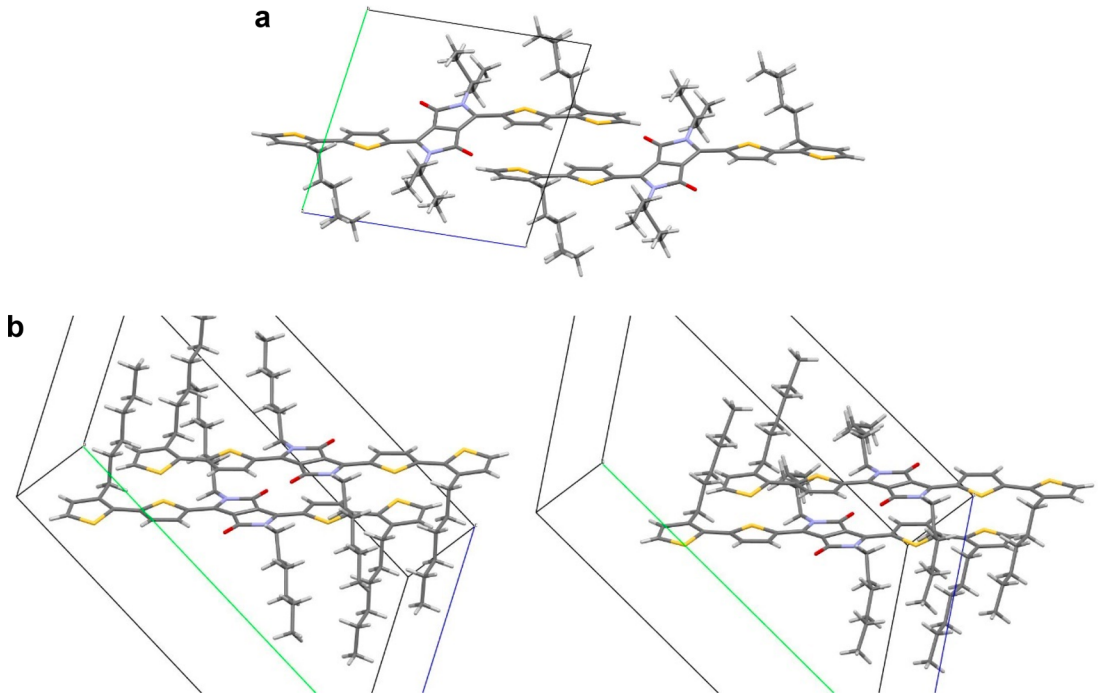

Figure 7. (a) Crystal structure of **2** viewed along the *a* axis showing two molecules in adjacent unit cells of which the bithiophene units are π-stacked. The slipping angle is 15.0°. (b) Crystal structure of **6** showing the π-stacking of two centrosymmetric molecules (**6′**) (left) and two noncentrosymmetric molecules (**6″**) (right). Separate panels are used for clarity. In both cases a molecule from an adjacent cell is shown. For **6′** and **6″**, π-stacking is similar to slipped cofacial arrangement and slipping angles of 45.4° for **6′** and 47.6° for **6″**.

Modeling Absorption Spectra in the Solid State. Because the π-overlap of neighboring ring systems depends on the cosine of the torsion angle, the effect of $\alpha = 152.9(1)°$ in **2** versus $\alpha, \alpha' \geq 173.0(4)°$ in **6** on the extent of π-conjugation is expected to be small. As a consequence, the spectra of solutions of **2** and **6** differ only marginally (Figure 2a,b). It is clear that the difference in torsion angles cannot explain the dramatic difference between the spectra of **1**−**4** and of **5**−**8** in thin films. The origin must be related to differences in intermolecular interactions, and it useful to attempt to rationalize these differences. For that we first consider the π-stacking motifs for **2** and **6** as they occur in the solid state.

In the crystal of **2**, the bithiophene unit π-stacks with bithiophene units of neighboring molecules (Figure 7a). Figure 7a clearly shows that the nonplanar conformation around the DPP unit and the sterically demanding 3-pentyl substituents cause that the DPP units are not participating in π-stacking. Considering that the transition dipole moment in **2** is largely oriented along the long axis of the molecule, the angle θ of the transition dipole moment of **2** and the intermolecular vector is 15.0° and much smaller than the magic angle of 54.7° such that the relative orientation of the two molecules formally corresponds to that of a J aggregate. The spectra of films of **2** might be consistent with that but do not clearly show the expected high intensity absorption at long wavelengths that is typical for J aggregates. In an analysis of point transition dipole moment interactions, we find the strongest interaction with the nearest neighbor along the *a* axis (+0.3 eV). In calculating these interactions, we used the experimental transition dipole moment estimated from the optical absorption. For interactions with other nearest neighbors along the crystal *b* and *c* axes, interaction energies are an order of magnitude smaller (+0.002 and −0.005 eV, respectively). Based on these interaction energies, one would expect H aggregate behavior, at strong variance with the experimental absorption spectrum for compound **2**.

The π-stacking of **6** in the solid state is dramatically different. π-Stacking of **6** occurs primarily via interactions between the **6′**-**6′** and **6″**-**6″** pairs of isomers (Figure 7b). As a consequence of its planar structure, molecules of **6′** and **6″** pack in a slipped cofacial arrangement (Figure 7b). The angle θ in this case is 45.4° for **6′** and 47.6° for **6″**, both slightly smaller than the magic angle of 54.7°. At the magic angle, the difference between H and J aggregates and the net coupling of transition dipole moments disappears, which would not give rise to rather complex spectra shown in Figure 2d. For this compound, the interaction energy between point transition dipole moments of neighboring molecules in the unit cell is −0.022 eV, while for molecules in adjacent cells it is −0.12 eV along the *a* axis, −0.001 eV along the *b* axis, and +0.003 eV along the *c* axis. Hence, the strongest interaction corresponds to molecules that are shown in Figure 7, for which the angle θ is pointing to a small preference for J aggregates. Again this result is not in agreement with the experiments, which clearly shows a peak of lower intensity at low energy.

Therefore, simple arguments based on nearest neighbor interactions, point transition dipole moments, and invoking J or H aggregation cannot explain the features seen in the absorption spectra of **2** and **6** in the solid state.

To explain the spectra, we consider that in the singly excited state of a molecular crystal, the individual molecular transition dipoles can couple, leading to a delocalized excited state with a transition dipole moment for the transition to the ground state that is much larger than for the isolated molecule. As a result of the formation of such a large transition dipole moment, the interaction between light and the delocalized oscillating transition charge density can be strong and may no longer be accurately described by perturbation theory. Instead, the

https://dx.doi.org/10.1021/acs.jpcc.0c07334
J. Phys. Chem. C 2020, 124, 25229−25238

electromagnetic and electronic degrees of freedom can be strongly coupled and a solution of the coupled equations of motion can be sought. Obviously such a solution combines the characteristics of a photon and an exciton and is known as a *polariton*.[55−57] The properties of this quasi-particle are encoded in its dispersion relation $k(\omega) = \omega n(\omega)$ with k the wavevector, $n(\omega)$ the refractive index, and ω the frequency. In principle, optical properties of the crystalline state such as reflectivity and transmittivity can be obtained from the dispersion relation. In the section below, we try to calculate the dispersion relation for crystals of **2** and **6**.

In zero order of a perturbative approach, we neglect the structural details of the crystal and treat all molecules as equal. For the crystals of **2** and **6**, this approach is aided by the fact that all molecules are oriented with their long axis in the same direction. Next we introduce the complex refractive index $\tilde{n}(\omega) = n(\omega) + i\omega(\omega)$. In lowest order, the absorption in index κ is taken to have a single sharp maximum around the frequency of the lowest allowed transition of the isolated molecule κ_D:

$$\kappa(\omega) = \frac{\pi}{2}\frac{{\omega_P}^2}{\omega_D}\delta(\omega - \omega_D) \tag{1}$$

where δ denotes the Dirac delta function. The normalization follows from the Thomas−Reiche−Kuhn sum rule:[58]

$$\int_0^\infty \omega\kappa(\omega)\,\mathrm{d}\omega = \frac{\pi}{4}{\omega_P}^2 \tag{2}$$

where ${\omega_P}^2$ represent the square of the plasma frequency:

$${\omega_P}^2 = \frac{Nq^2}{m_e} \tag{3}$$

N denotes the number density of molecules with oscillator strength q^2 and electron mass m_e. Finally, the Kramers−Kronig relation,[59,60] between the real and imaginary part of the refractive index:[61,62]

$$n(\omega) = 1 + \frac{2}{\pi}P\int_0^\infty \frac{\omega'\kappa(\omega')}{{\omega'}^2 - \omega^2}\,\mathrm{d}\omega' \tag{4}$$

with P indicating the principal value, yields the real part of the refractive index and implicitly also the dispersion relation:

$$n(\omega) = 1 + \frac{{\omega_P}^2}{{\omega_D}^2 - \omega^2} \tag{5}$$

Equation 5 can also be derived in a more elaborate manner by summing secondary radiation waves emitted by Lorentz dipole oscillators.[63] From this more involved approach, it becomes clear that eq 5 pertains to waves with their propagation direction perpendicular to the dipole axes with polarization parallel to the oscillators. Furthermore, eq 5 is part of a description involving the fully retarded Lorenz gauge for the electromagnetic field.

In a next iterative improvement upon eq 5, we want to consider structural details of the crystals. We note that in the crystal, the transition charge densities of neighboring molecules will interact, leading to a renormalization of the resonance frequencies. First we calculate the transition charge density by DFT for the lowest allowed S_0−S_1 electronic transition under the simplifying assumption that it can be described by an excitation of one electron from the HOMO to the LUMO (Figures S5 and S6, Supporting Information). The transition charge density is then approximated by a set of point charges located at the centers of the atoms in the molecule. The resulting charge densities are collected in Tables S2 and S3 (Supporting Information). Next we sum the interaction energies between point charges of different molecules using the Ewald method.[64,65] For the crystal of **6** with its three molecules in the unit cell, renormalized resonance energies are obtained by diagonalizing the 3 × 3 Hamilton matrix containing as the off-diagonal elements the summed interaction energies for each molecule in the unit cell. From the eigenvectors, a renormalized plasma frequency is calculated. The renormalized plasma and resonance frequencies depend on wavevector and frequency, resulting in eq 6:

$$k(\omega) = \omega\left(1 + \frac{{\omega_P}(k,\omega)^2}{{\omega_D}(k,\omega)^2 - \omega^2}\right) \tag{6}$$

Using a numerical procedure, we search for self-consistent solutions of eq 6 in terms of $k(\omega)$. We note that the intermolecular interactions are calculated including retardation in order to be consistent with the adopted Lorenz gauge in the zero-order approach. The inclusion retardation has the additional advantage that the contribution of surface charges induced at the boundary of the crystal on the local potential inside goes to zero in the limit of a macroscopic crystal. Hence the solution obtained is independent of the macroscopic shape of the crystal. The problems with the nonanalytic behavior of the unretarded dipole sums in the Coulomb gauge in the limit $k \to 0$ associated with surface charge can be avoided.[66−68]

The renormalized dispersion relations for the crystals of **2** and of **6** are shown in Figure 8. For **2**, the dispersion relation

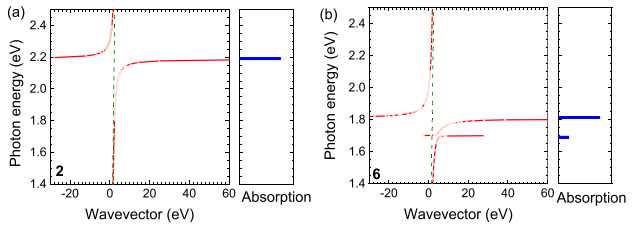

Figure 8. (a) Dispersion relation for crystalline **2** calculated from eq 6 for wavevectors perpendicular to the transition dipole moment using the crystal structure as input together ω_D = 2.25 eV from the onset of the solution absorption spectrum and ω_P = 0.73 eV using the number density of molecules from the X-ray crystal structure and the oscillator strength from the integrated solution spectrum.[69] The green dashed line shows the photon dispersion relation $k = \omega$. The right panel show a stylized absorption spectrum corresponding to the Kramers−Kronig transform of the dispersion relation. (b) Dispersion relation for crystalline **6** with ω_D = 2.07 eV and ω_P = 0.83 eV and corresponding absorption spectra.

shows a single divergence. Calculating $n(\omega) = k(\omega)/\omega$ and subsequent Kramers−Kronig transformation yields an absorption spectrum. This is essentially a stick spectrum because our treatment ignores coupling with vibrations, and so information on the band shape is fully absent. For **2**, we find a single resonance frequency at 2.19 eV. Thus, the calculations predict a small shift in resonance frequency in comparison to the isolated molecule in solution. This prediction is largely consistent with the experiment seen in Figure 2. For **6**, we predict two divergencies in the dispersion curve and, correspondingly, two resonance frequencies in absorption located at 1.81 and 1.70 eV. The resonance at 1.81 eV has a

https://dx.doi.org/10.1021/acs.jpcc.0c07334
J. Phys. Chem. C 2020, 124, 25229−25238

wider splitting between the positive and negative branch, and so the coupling between light and the mechanical motion at 1.81 eV must be considerably stronger than at 1.70 eV. Consequently, the absorption at 1.81 eV is predicted to be stronger than at 1.70 eV. Following Davydov,[70] for a crystal with three molecules in the unit cell, one expects at most three resonance frequencies. For the space group of the crystal at hand ($P\bar{1}(2)$), the factor group (C_i) has inversion symmetry. It follows then that of the three symmetry adapted combinations that can be made from the three molecular transition dipoles in the unit cell, one combination has no dipole strength because of its even symmetry under inversion. Hence symmetry considerations suggest only two allowed transitions. The experimental absorption spectrum for solid films of **6**, see Figure 2, shows two maxima, one at 2.22 eV and the other at 1.85 eV. Consistent with the predictions, the absorption at the low energy resonance has lower intensity.

CONCLUSION

Two sets of bis(bithiophene)-DPP molecules were synthesized to study the effect of α-branching of the alkyl side chains on the DPP unit on the optical properties. In both sets (**1**−**4** and **5**−**8**), the molecules differ by the absence or presence of additional *n*-hexyl side chains on the terminal thiophene rings in the 3′, 4′, or 5′ positions. The incorporation of α-branched 3-pentyl side chains in molecules **1**−**4** resulted in markedly different optical properties in absorption and emission in thin films compared to derivatives **5**−**8** with linear *n*-hexyl side chains on the DPP, while in solution, the spectral characteristics differ in a much more subtle way.

In the thin film, the optical absorption spectra of **5**−**8** show clear evidence of intermolecular interactions that result in a significant broadening of the absorption spectra compared to those in solution, exhibiting a long-wavelength absorption that is less intense than at shorter wavelengths. In contrast, for **1**−**4**, the spectra of solid films and solutions are much more alike apart from a small redshift and have somewhat more pronounced vibrational coupling. These different characteristics are also evident in fluorescence spectra, which show a very weak, broad emission for **5**−**8** and an almost molecular emission for **1**−**4**.

Crystals grown from **2** and **6** allowed for the determination of their crystal structures. The main difference is that due to the sterically congested 3-pentyl substituents, molecule **2** is nonplanar and exhibits a significant torsion angle for the bonds between DPP and thiophene. In contrast, molecule **6** is virtually planar. NMR spectroscopy in solution and DFT calculations confirm the characteristics of the crystal structures found and suggest that these are intrinsic properties of the molecules. The important result of the nonplanarity is a different three-dimensional packing in the solid state, because it affects the slip angle.[71] Whereas **2** crystallizes in a brick layer stacking mode with a slip angle of 15°, crystals of **6** grow in a slip stacking mode with a slip angle of 46.5 ± 1°. The α-branched side chains on DPP inhibit the DPP segment to π-stack in crystals of **2**. To explain the absorption spectra in the solid state, we approximated the transition charge density for the lowest allowed S_0−S_1 electronic transition as a HOMO to LUMO excitation by a set of point charges located at the centers of the atoms in the molecules and sum the interaction energies between point charges of different molecules in the crystal using the Ewald method. By solving the dispersion relation and performing a Kramers−Kronig transformation, an absorption spectrum could be obtained that represents the optical absorption of the molecules in the crystal. The results of the calculations match with the experimental observations in Figure 2c,d in the sense that for **2**, a single resonance frequency at 2.19 eV is obtained, while for **6** two transitions are predicted at 1.81 and 1.70 eV, with the lower-energy transition being less intense. As such a qualitative explanation has been reached.

ASSOCIATED CONTENT

Supporting Information

The Supporting Information is available free of charge at https://pubs.acs.org/doi/10.1021/acs.jpcc.0c07334.

Description of synthesis and characterization of the new molecules and details on the crystal structure determination of **2** and **6** (PDF)

Crystallographic data for **2** and **6** (CIF)

CheckCIF/PLATON report (PDF)

AUTHOR INFORMATION

Corresponding Authors

Stefan C. J. Meskers − *Molecular Materials and Nanosystems & Institute for Complex Molecular Systems, Eindhoven University of Technology, 5600 MB Eindhoven, The Netherlands;* orcid.org/0000-0001-9236-591X; Email: s.c.j.meskers@tue.nl

René A. J. Janssen − *Molecular Materials and Nanosystems & Institute for Complex Molecular Systems, Eindhoven University of Technology, 5600 MB Eindhoven, The Netherlands; Dutch Institute for Fundamental Energy Research, 5612 AJ Eindhoven, The Netherlands;* orcid.org/0000-0002-1920-5124; Email: r.a.j.janssen@tue.nl

Authors

Bart W. H. Saes − *Molecular Materials and Nanosystems & Institute for Complex Molecular Systems, Eindhoven University of Technology, 5600 MB Eindhoven, The Netherlands*

Martin Lutz − *Utrecht University, Crystal and Structural Chemistry, Bijvoet Centre for Biomolecular Research, Faculty of Science, 3584 CH Utrecht, The Netherlands*

Martijn M. Wienk − *Molecular Materials and Nanosystems & Institute for Complex Molecular Systems, Eindhoven University of Technology, 5600 MB Eindhoven, The Netherlands*

Complete contact information is available at: https://pubs.acs.org/10.1021/acs.jpcc.0c07334

Notes

The authors declare no competing financial interest.

CCDC 2013158 (compound **2**) and 2013159 (compound **6**) contain the supplementary crystallographic data for this paper. These data can be obtained free of charge from The Cambridge Crystallographic Data Centre via www.ccdc.cam.ac.uk/structures.

ACKNOWLEDGMENTS

We acknowledge funding from the European Research Council (Grant Agreement No. 339031) and the NWO Spinoza prize awarded to R. A. J. Janssen by The Netherlands Organization for Scientific Research (NWO), and the Ministry of Education,

Culture and Science (Gravity Program 024.001.035). The X-ray diffractometer has been financed by NWO.

REFERENCES

(1) Wallquist, O.; Lenz, R. 20 years of DPP pigments - future perspectives. *Macromol. Symp.* **2002**, *187*, 617−630.
(2) Qu, S.; Tian, H. Diketopyrrolopyrrole (DPP)-based materials for organic photovoltaics. *Chem. Commun.* **2012**, *48*, 3039−3051.
(3) Nielsen, C. B.; Turbiez, M.; McCulloch, I. Recent advances in the development of semiconducting DPP-containing polymers for transistor applications. *Adv. Mater.* **2013**, *25*, 1859−1880.
(4) Naik, M. A.; Patil, S. Diketopyrrolopyrrole-based conjugated polymers and small molecules for organic ambipolar transistors and solar cells. *J. Polym. Sci., Part A: Polym. Chem.* **2013**, *51*, 4241−4260.
(5) Li, Y.; Sonar, P.; Murphy, L.; Hong, W. High mobility diketopyrrolopyrrole (DPP)-based organic semiconductor materials for organic thin film transistors and photovoltaics. *Energy Environ. Sci.* **2013**, *6*, 1684−1710.
(6) Yi, Z.; Wang, S.; Liu, Y. Design of high-mobility diketopyrrolopyrrole-based π-conjugated copolymers for organic thin-film transistors. *Adv. Mater.* **2015**, *27*, 3589−3606.
(7) Grzybowski, M.; Gryko, D. T. Diketopyrrolopyrroles: Synthesis, reactivity, and optical properties. *Adv. Opt. Mater.* **2015**, *3*, 280−320.
(8) Li, W.; Hendriks, K. H.; Wienk, M. M.; Janssen, R. A. J. Diketopyrrolopyrrole polymers for organic solar cells. *Acc. Chem. Res.* **2016**, *49*, 78−85.
(9) Tang, A.; Zhan, C.; Yao, J.; Zhou, E. Design of diketopyrrolopyrrole (DPP)-based small molecules for organic-solar-cell applications. *Adv. Mater.* **2017**, *29*, 1600013.
(10) Patil, Y.; Misra, R. Rational molecular design towards NIR absorption: efficient diketopyrrolopyrrole derivatives for organic solar cells and photothermal therapy. *J. Mater. Chem. C* **2019**, *7*, 13020−13031.
(11) Jiang, X.; Wang, L.; Tang, H.; Cao, D.; Chen, W. Diketopyrrolopyrrole: An emerging phototherapy agent in fighting cancer. *Dyes Pigm.* **2020**, *181*, 108599.
(12) Liu, Q.; Bottle, S. E.; Sonar, P. Developments of diketopyrrolopyrrole-dye-based organic semiconductors for a wide range of applications in electronics. *Adv. Mater.* **2020**, *32*, 1903882.
(13) Leventis, A.; Royakkers, J.; Rapidis, A. G.; Goodeal, N.; Corpinot, M. K.; Frost, J. M.; Bučar, D.-K.; Blunt, M. O.; Cacialli, F.; Bronstein, H. Highly luminescent encapsulated narrow bandgap polymers based on diketopyrrolopyrrole. *J. Am. Chem. Soc.* **2018**, *140*, 1622−1626.
(14) Naik, M. A.; Venkatramaiah, N.; Kanimozhi, C.; Patil, S. Influence of side-chain on structural order and photophysical properties in thiophene based diketopyrrolopyrroles: A systematic study. *J. Phys. Chem. C* **2012**, *116*, 26128−26137.
(15) Gevaerts, V. S.; Herzig, E. M.; Kirkus, M.; Hendriks, K. H.; Wienk, M. M.; Perlich, J.; Müller-Buschbaum, P.; Janssen, R. A. J. Influence of the position of the side chain on crystallization and solar cell performance of DPP-based small molecules. *Chem. Mater.* **2014**, *26*, 916−926.
(16) Más-Montoya, M.; Janssen, R. A. J. The effect of H- and J-aggregation on the photophysical and photovoltaic properties of small thiophene-pyridine-DPP molecules for bulk-heterojunction solar cells. *Adv. Funct. Mater.* **2017**, *27*, 1605779.
(17) Manley, E. F.; Harschneck, T.; Eastham, N. D.; Leonardi, M. J.; Zhou, N.; Strzalka, J.; Chang, R. P. H.; Chen, L. X.; Marks, T. J. Side chain and solvent direction of film morphology in small-molecule organic solar materials. *Chem. Mater.* **2019**, *31*, 8308−8319.
(18) He, T.; Leowanawat, P.; Burschka, C.; Stepanenko, V.; Stolte, M.; Würthner, F. Impact of 2-ethylhexyl stereoisomers on the electrical performance of single-crystal field-effect transistors. *Adv. Mater.* **2018**, *30*, 1804032.
(19) Klebe, G.; Graser, F.; Hadicke, E.; Berndt, J. Crystallochromy as a solid-state effect: correlation of molecular conformation, crystal packing and colour in perylene-3,4:9,10-bis(dicarboximide) pigments. *Acta Crystallogr., Sect. B: Struct. Sci.* **1989**, *45*, 69−77.
(20) Kazmaier, P. M.; Hoffmann, R. A theoretical study of crystallochromy. Quantum interference effects in the spectra of perylene pigments. *J. Am. Chem. Soc.* **1994**, *116*, 9684−9691.
(21) Mizuguchi, J. Correlation between crystal and electronic structures in diketopyrrolopyrrole pigments as viewed from exciton coupling effects. *J. Phys. Chem. A* **2000**, *104*, 1817−1821.
(22) Mizuguchi, J.; Rochat, A. C. A new near-infrared photoreceptor based on 1,4-dithioketo-3,6-diphenylpyrrolo[3,4-c]-pyrrole. *J. Imaging Sci.* **1988**, *32*, 135−140.
(23) Liu, J.; Walker, B.; Tamayo, A.; Zhang, Y.; Nguyen, T.-Q. Effects of heteroatom substitutions on the crystal structure, film formation, and optoelectronic properties of diketopyrrolopyrrole-based materials. *Adv. Funct. Mater.* **2013**, *23*, 47−56.
(24) Liu, J.; Zhang, Y.; Phan, H.; Sharenko, A.; Moonsin, P.; Walker, B.; Promarak, V.; Nguyen, T.-Q. Effects of stereoisomerism on the crystallization behavior and optoelectrical properties of conjugated molecules. *Adv. Mater.* **2013**, *25*, 3645−3650.
(25) Calvo-Castro, J.; Warzecha, M.; Kennedy, A. R.; McHugh, C. J.; McLean, A. J. Impact of systematic structural variation on the energetics of π-π stacking interactions and associated computed charge transfer integrals of crystalline diketopyrrolopyrroles. *Cryst. Growth Des.* **2014**, *14*, 4849−4858.
(26) Dhar, J.; Venkatramaiah, N.; A, A.; Patil, S. Photophysical, electrochemical and solid state properties of diketopyrrolopyrrole based molecular materials: importance of the donor group. *J. Mater. Chem. C* **2014**, *2*, 3457−3466.
(27) Hartnett, P. E.; Margulies, E. A.; Mauck, C. M.; Miller, S. A.; Wu, Y.; Wu, Y.-L.; Marks, T. J.; Wasielewski, M. R. Effects of crystal morphology on singlet exciton fission in diketopyrrolopyrrole thin films. *J. Phys. Chem. B* **2016**, *120*, 1357−1366.
(28) Mauck, C. M.; Hartnett, P. E.; Margulies, E. A.; Ma, L.; Miller, C. E.; Schatz, G. C.; Marks, T. J.; Wasielewski, M. R. Singlet fission via an excimer-like intermediate in 3,6-bis(thiophen-2-yl)-diketopyrrolopyrrole derivatives. *J. Am. Chem. Soc.* **2016**, *138*, 11749−11761.
(29) Yoon, W. S.; Kim, D. W.; Park, J.-M.; Cho, I.; Kwon, O. K.; Whang, D. R.; Kim, J. H.; Park, J.-H.; Park, S. Y. A novel bis-lactam acceptor with outstanding molar extinction coefficient and structural planarity for donor-acceptor type conjugated polymer. *Macromolecules* **2016**, *49*, 8489−8497.
(30) Calvo-Castro, J.; Maczka, S.; Thomson, C.; Morris, G.; Kennedy, A. R.; McHugh, C. J. Twist and shout: a surprising synergy between aryl and N-substituents defines the computed charge transport properties in a series of crystalline diketopyrrolopyrroles. *CrystEngComm* **2016**, *18*, 9382−9390.
(31) Loser, S.; Lou, S. J.; Savoie, B. M.; Bruns, C. J.; Timalsina, A.; Leonardi, M. J.; Smith, J.; Harschneck, T.; Turrisi, R.; Zhou, N.; et al. Systematic evaluation of structure-property relationships in hetero-acene - diketopyrrolopyrrole molecular donors for organic solar cells. *J. Mater. Chem. A* **2017**, *5*, 9217−9232.
(32) Mauck, C. M.; Bae, Y. J.; Chen, M.; Powers-Riggs, N.; Wu, Y.-L.; Wasielewski, M. R. Charge-transfer character in a covalent diketopyrrolopyrrole dimer: implications for singlet fission. *ChemPhotoChem.* **2018**, *2*, 223−233.
(33) Genevaz, N.; Chavez, P.; Untilova, V.; Boeglin, A.; Bailly, C.; Karmazin, L.; Biniek, L. Tuning crystallochromism in diketopyrrolo-pyrrole-co-thieno[3,2-b]thiophene derivatives by the architecture of their alkyl side chains. *J. Mater. Chem. C* **2018**, *6*, 9140−9151.
(34) Hume, P. A.; Monks, J. P.; Pop, F.; Davies, E. S.; MacKenzie, R. C. I.; Amabilino, D. B. Self-assembly of chiral-at-end diketopyrrolo-pyrroles: symmetry dependent solution and film optical activity and photovoltaic performance. *Chem. - Eur. J.* **2018**, *24*, 14461−14469.
(35) Smith, M. B.; Michl, J. Singlet Fission. *Chem. Rev.* **2010**, *110*, 6891−6936.
(36) Greyson, E. C.; Vura-Weis, J.; Michl, J.; Ratner, M. A. Maximizing singlet fission in organic dimers: theoretical investigation of triplet yield in the regime of localized excitation and fast coherent electron transfer. *J. Phys. Chem. B* **2010**, *114*, 14168−14177.

https://dx.doi.org/10.1021/acs.jpcc.0c07334
J. Phys. Chem. C 2020, 124, 25229−25238

(37) Johnson, J. C.; Nozik, A. J.; Michl, J. The role of chromophore coupling in singlet fission. *Acc. Chem. Res.* **2013**, *46*, 1290−1299.
(38) Mukhopadhyay, T.; Musser, A. J.; Puttaraju, B.; Dhar, J.; Friend, R. H.; Patil, S. Is the chemical strategy for imbuing "polyene" character in diketopyrrolopyrrole-based chromophores sufficient for singlet fission? *J. Phys. Chem. Lett.* **2017**, *8*, 984−991.
(39) Miller, C. E.; Wasielewski, M. R.; Schatz, G. C. Modeling singlet fission in rylene and diketopyrrolopyrrole derivatives: The role of the charge transfer state in superexchange and excimer formation. *J. Phys. Chem. C* **2017**, *121*, 10345−10350.
(40) Mauck, C. M.; Hartnett, P. E.; Wu, Y.-L.; Miller, C. E.; Marks, T. J.; Wasielewski, M. R. Singlet fission within diketopyrrolopyrrole nanoparticles in water. *Chem. Mater.* **2017**, *29*, 6810−6817.
(41) Shen, L.; Tang, Z.; Wang, X.; Liu, H.; Chen, Y.; Li, X. Effects of aromatic substituents on the electronic structure and excited state energy levels of diketopyrrolopyrrole derivatives for singlet fission. *Phys. Chem. Chem. Phys.* **2018**, *20*, 22997.
(42) Levine, A. M.; Schierl, C.; Basel, B. S.; Ahmed, M.; Camargo, B. A.; Guldi, D. M.; Braunschweig, A. B. Singlet fission in combinatorial diketopyrrolopyrrole-rylene supramolecular films. *J. Phys. Chem. C* **2019**, *123*, 1587−1595.
(43) Krishnapriya, K. C.; Roy, P.; Puttaraju, B.; Salzner, U.; Musser, A. J.; Jain, M.; Dasgupta, J.; Patil, S. Spin density encodes intramolecular singlet exciton fission in pentacene dimers. *Nat. Commun.* **2019**, *10*, 33.
(44) Kirkus, M.; Janssen, R. A. J.; Meskers, S. C. J. Intramolecular excimer formation between 3,6-di(thiophen-2-yl)pyrrolo[3,4-c]-pyrrole-1,4(2H,5H)-dione chromophoric groups linked by a flexible alkyl spacer. *J. Phys. Chem. A* **2013**, *117*, 4828−4837.
(45) Avcibaşi, N.; Smet, M.; Metten, B.; Dehaen, W.; De Schryver, F. C.; Bultynck, G.; Callewaert, G.; De Smedt, H.; Missiaen, L.; Boens, N. Synthesis and in vitro evaluation of dioxopyrrolopyrroles as potential low-affinity fluorescent Ca^{2+} indicators. *Int. J. Photoenergy* **2004**, *6*, 159−167.
(46) Te Velde, G.; Bickelhaupt, F. M.; Baerends, E. J.; Fonseca Guerra, C.; van Gisbergen, S. J. A.; Snijders, J. G.; Ziegler, T. Chemistry with ADF. *J. Comput. Chem.* **2001**, *22*, 931−967.
(47) Wang, Y.; Huang, Q.; Liu, Z.; Li, H. A perfluorohexyl containing diketopyrrolopyrrole (DPP) small molecule for high performance ambipolar transistors with balanced hole and electron mobilites. *RSC Adv.* **2014**, *4*, 29509−29513.
(48) Pop, F.; Humphreys, J.; Schwarz, J.; Brown, L.; Van den Berg, A.; Amabilino, D. B. Towards more sustainable synthesis of diketopyrrolopyrroles. *New J. Chem.* **2019**, *43*, 5783−5790.
(49) Saes, B. W. H.; Wienk, M. M.; Janssen, R. A. J. The effect of α-branched side chains on the structural and opto-electronic properties of poly(diketopyrrolopyrrole-alt-terthiophene). *Chem. Eur. J.* **2020**, DOI: 10.1002/chem.202001722.
(50) Mishra, S. P.; Palai, A. K.; Patri, M. Synthesis and characterization of soluble narrow band gap conducting polymers based on diketopyrrolopyrrole and propylenedioxythiophenes. *Synth. Met.* **2010**, *160*, 2422−2429.
(51) Zheng, T.; Schneider, A. M.; Yu, L. Stille polycondensation: a versatile synthetic approach to functional polymers. In *Synthetic Methods for Conjugated Polymers and Carbon Materials*, 1st ed.; Leclerc, M., Morin, J.-F., Eds.; Wiley-VCH Verlag GmbH & CoKGaA: Weinheim, Germany, 2017; pp 1−58.
(52) Liu, Y.; Xiang, N.; Feng, X.; Shen, P.; Zhou, W.; Weng, C.; Zhao, B.; Tan, S. Thiophene-linked porphyrin derivatives for dye-sensitized solar cells. *Chem. Commun.* **2009**, 2499−2501.
(53) Meskers, S. C. J.; Janssen, R. A. J.; Haverkort, J. E. M.; Wolter, J. H. Relaxation of photo-excitations in films of oligo- and poly-(para-phenylene vinylene) derivatives. *Chem. Phys.* **2000**, *260*, 415−439.
(54) Spano, F. C.; Silva, C. H- and J-aggregate behavior in polymeric semiconductors. *Annu. Rev. Phys. Chem.* **2014**, *65*, 477−500.
(55) Huang, K. On the interaction between the radiation field and ionic crystals. *Proc. R. Soc. A* **1951**, *208*, 352−365.
(56) Pekar, S. I. Theory of electromagnetic waves in a crystal with excitons. *J. Phys. Chem. Solids* **1958**, *5*, 11−22.
(57) Hopfield, J. J. Theory of the contribution of excitons to the complex dielectric constant of crystals. *Phys. Rev.* **1958**, *112*, 1555−1565.
(58) Smith, D. Y. Dispersion theory, sum rules, and their application to analysis of optical data. In *Handbook of Optical Constants of Solids*; Palik, E. D., Ed.; Academic Press: San Diego, CA, 1985; Vol. *1*, pp 35−68.
(59) Nussenzveig, H. M. *Causality and Dispersion Relations*; Academic Press: New York, 1972.
(60) Ashcroft, N. W.; Mermin, N. D. *Solid State Physics*; Brook/Cole Publishing, Belmont, CA, 1976.
(61) Hale, G. M.; Querry, M. R. Optical constants of water in the 200-nm to 200-μm wavelength region. *Appl. Opt.* **1973**, *12*, 555−563.
(62) Moffitt, W.; Moscowitz, A. Optical activity in absorbing media. *J. Chem. Phys.* **1959**, *30*, 648−660.
(63) Meskers, S. C. J.; Lakhwani, G. Reflection of light by anisotropic molecular crystals including exciton-polaritons and spatial dispersion. *J. Chem. Phys.* **2016**, *145*, 194703.
(64) Ewald, P. P. The calculation of optical and electrostatic grid potential. *Ann. Phys.* **1921**, *369*, 253.
(65) Borwein, J.; Glasser, M.; McPhedran, R.; Wan, J.; Zucker, I. *Lattice Sums Then and Now*; Encyclopedia of Mathematics and Its Applications; Cambridge University Press: Cambridge, U.K., 2013.
(66) Cohen, M. H.; Keffer, F. Dipolar sums in the primitive cubic lattices. *Phys. Rev.* **1955**, *99*, 1128−1134.
(67) Philpott, M. R.; Lee, J. W. Some remarks on the calculation and use of retarded and static dipole sums in molecular exciton theory. *J. Chem. Phys.* **1973**, *58*, 595−602.
(68) Smith, E. R. Electrostatic potentials in systems periodic in one, two, and three dimensions. *J. Chem. Phys.* **2008**, *128*, 174104.
(69) Michl, J.; Thulstrup, E. W. *Spectroscopy with Polarized Light*; VCH Publishers: New York, 1986.
(70) Davydov, A. S. *Theory of Molecular Excitons*; Springer: Boston, MA, 1971.
(71) Yao, Z.-F.; Wang, J.-Y.; Pei, J. Control of π-π stacking via crystal engineering in organic conjugated small molecule crystals. *Cryst. Growth Des.* **2018**, *18*, 7−15.

https://dx.doi.org/10.1021/acs.jpcc.0c07334
J. Phys. Chem. C 2020, 124, 25229−25238